Article:
Wang, Y.-S., Provis, J.L. orcid.org/0000-0003-3372-8922 and Dai, J.-G. (2018) Role of soluble aluminum species in the activating solution for synthesis of silico-aluminophosphate geopolymers. Cement and Concrete Composites, 93. pp. 186-195. ISSN 0958-9465

https://doi.org/10.1016/j.cemconcomp.2018.07.011

Role of soluble aluminum species in the activating solution for synthesis of silico-aluminophosphate geopolymers

Yan-Shuai Wang[1], John L. Provis[2*] and Jian-Guo Dai[3*]

[1] PhD Candidate, Department of Civil and Environmental Engineering, The Hong Kong Polytechnic University, Hong Kong, China

[2] Professor, Department of Materials Science and Engineering, University of Sheffield, Sir Robert Hadfield Building, Portobello Street, Sheffield, UK. Corresponding author: j.provis@sheffield.au.uk

[3] Professor, Department of Civil and Environmental Engineering, The Hong Kong Polytechnic University, Hong Kong, China. Corresponding author: cejgdai@polyu.edu.hk

Abstract:

An aluminosilicate precursor, such as metakaolin, can be transformed into a cement-like geopolymer binder via a phosphate activation approach. This paper identifies the effect of the addition of aluminum species into the phosphate activating solution on the formation of such geopolymers, from the fresh to the hardened state. Activating solutions with Al/P molar ratios of 0, 0.1, and 0.3 were prepared by blending monoaluminum phosphate (MAP) and orthophosphoric acid (OPA). The rheological properties, fluidity, and setting times of the fresh geopolymer pastes and the compressive strength of the hardened geopolymer matrices were studied. Liquid-state ^{27}Al and ^{31}P nuclear magnetic resonance (NMR) measurements for the chemical environments of Al and P, and spectroscopic, thermal, and microscopic analyses revealed that the soluble aluminum in the phosphate activating solution played an important role during the geopolymerization process. Seeding of aluminum species through inclusion in the activating solution allowed a rapid sol/gel transition that improved the rheological properties and setting time of the fresh geopolymer pastes at ambient temperature. However, although the increased concentration of aluminum phosphate oligomers promoted by the soluble aluminum addition contributed to the formation of a compact matrix with high early strength, it hinders the ongoing reaction of metakaolin in the later period, which has a detrimental influence on ongoing strength development beyond 7 days of curing.

Keywords:

Silico-aluminophosphate geopolymer; Metakaolin; Phosphate activating solution; Soluble aluminum; Setting time; Rheology

1. Introduction

The term “geopolymer” is often used to describe an inorganic polymeric material with polymer-like poly-aluminosilicate chains or networks [1]. Its formation is based on the reaction between an aluminosilicate precursor and an activating solution, which promotes the dissolution of the particulate precursor, and the consequent polycondensation of high-connectivity silicate networks as binding phases to form a hardened material [2, 3]. Compared to Portland cement, the geopolymer material is becoming a strong competitor due to its attractive features of sustainability and durability [4], especially when life cycle assessment (LCA)-based mix design technology of geopolymers is effectively applied [5]. Besides, geopolymer-made products can exhibit excellent thermal stability or fire-resistance [1], mechanical performance [6] and chemical anticorrosion properties (e.g., against acid, sulfate and chloride attack) [7].

The formation of geopolymer binders is conventionally based on alkali activation of aluminosilicates, where the hydroxide ions enable the dissolution of the solid aluminosilicate precursors to form isolated aluminate and silicate anions, and the elevated concentrations of these species in the aqueous state then drive polymerization, also involving hydrated cations to charge-balance, by reforming the aluminosilicate bonds [8]. However, an alternative activation approach for the aluminosilicate sources is phosphate activation [9, 10], which involves an analogous acid-activated reaction process involving phosphoric acid. The mechanism of phosphate-activated geopolymerization starts with the dealumination of the aluminosilicate source (i.e., dealumination reaction) into the acidic aqueous environment, following the polycondensation of free aluminate, silicate, and phosphate units to generate Si-O-Al, Si-O-P and/or Al-O-P bonds in silico-alumino-phosphate (S-A-P) gels [11, 12]; the structures of these gels are far from fully understood, and the chemical details of the mechanisms involved require further investigation.

The strong monolithic product of the phosphate activation of an aluminosilicate source, such as metakaolin, is sometimes termed a phosphate-based geopolymer [10, 13]. This reaction occurs in an acidic or low-alkaline medium environment in which a phosphate or phosphoric acid solution, rather than the alkali-silicate used in conventional geopolymers, chemically activates the aluminosilicate precursors to yield a compact geopolymer matrix with a condensed structure of silico-alumino-phosphate linkages [14, 15]. It has been claimed that the newly formed Al-O-P linkages could balance the charge caused by changes in the chemical environment of

aluminum [16], as is also observed in the synthesis of charge-neutral crystalline zeolite-like aluminophosphate and silico-alumino-phosphate frameworks [17]. Thus, a charge balance within the molecular structure is achieved without the involvement of monovalent cations. The above mechanisms create a silico-aluminophosphate geopolymer with low efflorescence and dielectric loss features, which are difficult to achieve in alkali-aluminosilicate geopolymers [16, 18].

Previous investigations on silico-aluminophosphate geopolymers [22-24] indicated that thermal curing (e.g., under sealed conditions at 60°C or 80°C) was usually needed to achieve fast setting and high early strength. This curing method can be accepted for precast geopolymer products but may impose difficulty in on-site operations, especially for larger-scale engineering applications. Thermal curing also consumes a significant amount of energy. To obtain an ambient-temperature hardening mechanism in alkali-activated geopolymers, soluble silicate is generally introduced in the alkaline activating solution because a high concentration of dissolved silicate can facilitate a rapid sol/gel transition that leads to the development of a compact matrix with useful early strength [25, 26]. The addition of a small dose of $NaAlO_2$ into an alkaline activating solution was also reported to improve the workability of the paste and accelerate the growth of the network structure of the formed geopolymer matrix [27].

Following these findings for alkaline systems, this study explores the potential to use a corresponding mechanism to improve the early-age characteristics of acidic geopolymers. A second aluminate source, in addition to the aluminosilicate source, is explored in this study as an additive to the phosphate activating solution. It is expected that the aluminum phosphate oligomers which form in a low-pH environment can modify the properties of fresh phosphate-based geopolymer paste and its hardened matrix. Aluminum and phosphorus generally exist in the free state at a pH of less than 3, and form aluminophosphate phases when the pH is increased [28]. Therefore, the addition of soluble aluminum may accelerate geopolymerization in the early stage of reaction to achieve an applicable setting time and early strength. A conceptual scheme for the reaction of an aluminosilicate source activated by alkali and phosphate to synthesize alkali-aluminosilicate and silico-aluminophosphate geopolymers, respectively, is displayed in Fig. 1, which illustrates the activating solution-accelerated formation processes from an aluminosilicate source to a geopolymer.

In this study, to assess the effectiveness of the addition of soluble aluminum species into a

phosphate activating solution for synthesizing geopolymers, various contents of soluble aluminum source were introduced, with the aim of modifying the setting time and rheological properties of the fresh geopolymer pastes at room temperature. The effects of the soluble aluminum species on the molecular structure of the resulting fresh and hardened geopolymer pastes were elaborated by liquid-state nuclear magnetic resonance (NMR) spectroscopy, other spectroscopic and thermal analyses. Microstructural features of the hardened geopolymer pastes as a function of Al addition were also explored by scanning electron microscopy (SEM) and mercury intrusion porosimetry (MIP).

2. Experimental

2.1 Materials and mix proportions

The phosphate-based geopolymer pastes were formulated to achieve designed molar ratios of silicon, aluminum and phosphorus. Metakaolin (MK) (KAOPOZZ, Chaopai Kaolin Co., Ltd., China) was used as the aluminosilicate source. The composition of MK was detected by X-ray fluorescence, on an ignited mass basis (LOI: 4.1%), as SiO_2 (51.1%), Al_2O_3 (46.8%), TiO_2 (0.8%), Fe_2O_3 (0.5%), CaO (0.2%), SO_3 (0.2%), and others (0.4%). The phosphate activating solution was prepared using orthophosphoric acid H_3PO_4 (OPA, 85 wt.% in H_2O, Ajax Finechem Laboratory Chemicals), liquid monoaluminum phosphate (MAP, $Al(H_2PO_4)_3$, 61.3 wt.% in H_2O, Xianju Litian Chemical Co. Ltd.), and deionized water. Three soluble aluminum contents (i.e., Al/P molar ratios of 0, 0.1, and 0.3) in the activating solutions were designed to represent control, low-content aluminum and high-content aluminum groups. The MAP supplied the soluble aluminum species in the activating solution, and had little influence on the initial pH value (as shown in Table 1). Silico-aluminophosphate geopolymers with a constant H_2O/MK mass ratio of 0.40 and a fixed Si/P molar ratio of 2.75 were produced by mixing the activating solution with the MK particles. As listed in Table 1, six different mix proportions were used, although the mixes A0-0.5, A1-0.5, and A2-0.5 were used only for tests of rheological properties.

OPA, MAP, and deionized water were fully blended in the specified proportions and cooled down to room temperature for use as the activating solutions, which were then mechanically homogenized with the MK particles for 5 min to form fresh geopolymer pastes. Before casting into 40×40×40 mm plastic molds, the respective rheological and flow properties of the fresh

geopolymer pastes and their initial and final setting times were measured. The hardened geopolymer pastes were demolded 48 hours after casting, and cured in moist conditions (95% to 100% relative humidity) at room temperature for specified periods.

2.2 Test methods

The characterization of the fresh geopolymer pastes was performed as follows:

(1) A rotational and oscillatory rheometer (Anton Paar MC302) equipped with a parallel-plate measuring system (maximum torque, 200 mN·m) was applied to measure the rheological properties of the fresh geopolymer pastes at a temperature of 25 ℃ by monitoring the evolution of shear stress (Pa) and viscosity (Pa·s) under shear rates ranging from 0.01 to 100 s^{-1}. The solid volume fractions of the geopolymer pastes with the two H_2O/MK ratios (0.4 and 0.5) were about 0.78 and 0.70, respectively, to ensure that the paste displayed a yield stress [29].

(2) The macroscopic fluidity of the fresh geopolymer pastes was determined by a mini-cone slump flow test setup [30] with an upper diameter of 36 mm, lower diameter of 60 mm, and height of 60 mm.

(3) The initial and final setting times of the geopolymers were determined using a Vicat apparatus according to BS EN 196-3: 2005.

(4) The liquid-state ^{31}P and ^{27}Al NMR spectra for the MAP and activating solutions were obtained using a Bruker 400 spectrometer at ambient temperature. The spectrometer frequencies for ^{31}P and ^{27}Al nuclei were 202.47 and 130.33 MHz, respectively. The corresponding recycle delays applied were 6 and 5 s, with 90º pulse durations of 8 and 2 μs, respectively. The chemical shifts of ^{31}P were expressed in ppm relative to the OPA, and the ^{27}Al resonances were referenced to a 1.0 mol/L $AlCl_3$ solution.

The compressive strength of the hardened geopolymer pastes was assessed before the spectroscopic, thermal, and microstructural analyses:

(1) The compressive strength of the 40-mm geopolymer paste cubes was measured after 3, 7, 14, and 28 days of curing by a mechanical testing instrument (Testometric CXM 500-50 kN) with a loading rate of 0.8 kN/s (about 0.5 MPa/s) following the guidance of ASTM C109/C109M-16a for load application.

(2) The crushed samples were then manually ground for crystalline phase analysis by X-ray diffractometry (XRD, Rigaku SmartLab) with a 9 kW Cu-Kα radiation source (λ=1.5406 Å)

and a scanning step of 0.02° (2□□.

(3) Simultaneous thermal analysis under an argon atmosphere (Thermo plus EVO2, Rigaku) was performed to analyze the thermal decomposition and phase transition behaviors of the hardened pastes, at a heating rate of 10 ^{o}C min^{-1}.

(4) The microstructural features were characterized by SEM (JEOL, JSM-6490) with energy-dispersive X-ray spectroscopy (EDS, Oxford INCA Energy 250). An acceleration voltage of 20 kV was applied. Before the microscopic measurement, the samples were desiccated (60 ℃ for 24 h) and surface coated with gold sputter.

(5) The pore size distribution of the samples was assessed by MIP (Micromeritics AutoPore IV9500). A geometrical model based on the Washburn equation, as shown in Eq. (1), was applied to determine the pore diameter.

$$D = -4\gamma\cos\theta / P \quad (1)$$

where, D (m) is the calculated pore diameter, γ (N/m) is the surface tension, θ (°) is the contact angle between mercury and pore wall, and P (Pa) is the applied pressure. The surface tension (γ) and contact angle (θ) selected in this study were 0.485 N/m and 140°, respectively. The applied pressure (P) ranged from 0.007 to 207 M Pa.

3. Results and Discussion

3.1 Fresh geopolymer pastes

3.1.1 Rheology

The Bingham model (Eq. (2)) is often used to approximate the rheological behavior of a hydraulic or geopolymer cement paste in terms of the shear stress-shear rate relationship over a specific range [31, 32]:

$$\tau = \tau_0 + \eta_0\gamma \quad (2)$$

where τ (Pa) is the shear stress, γ (s^{-1}) is the shear rate, and τ_0 (Pa) and η_0 (Pa·s) are the yield stress and plastic viscosity, respectively.

In particulate pastes, the viscosity and yield stress are controlled by colloidal interactions due to electrostatic and van der Waals forces between particles (the MK particles in this case), viscous forces in the interstitial liquid between particles (the activating solution in this case),

and direct contact forces [29].

Figure 2 plots the evolution of the rheological characteristics of the fresh geopolymer pastes, measured as a function of shear rate from 0.01 to 100 s^{-1}. The data shows that the Bingham model provides a reasonable – although not perfect – description of the rheological characteristics of these pastes. There is some deviation from Bingham behavior at the very beginning of the test, which may be related to thixotropic behavior as the MK particles are far from spherical and can thus cause complexities in time-dependent as well as shear-dependent rheology. Comparing between the various samples, it is seen that the presence of more Al species can promote a lower yield stress in the fresh phosphate-based geopolymer paste with a H_2O/MK ratio of 0.4 (i.e., A1-0.4 and A2-0.4). The geopolymer paste prepared using the Al-free activating solution at low water content (i.e., A0-0.4) was beyond the measurement range of the rheometer because of its high stickiness. The yield stress of the A1-0.4 and A2-0.4 pastes as estimated using the Bingham model reached 500 (±150) and 800 (±200) Pa, respectively, where the quoted error bounds on the yield stress values reflect the uncertainty introduced by the use of different sections of the flow curves to determine the yield stress via Eq. (2). The addition of a higher dose of Al to the activating solution (A2-0.4) gave a lower yield stress, and according to the Bingham model fitting results (i.e., the slope of fitting curves), the geopolymer paste with an Al/P molar ratio of 0.3 has a lower viscosity compared to A1-0.4 geopolymer paste. The Al species in the activating solution acted to some extent as a plasticizer, enabling the geopolymer paste to obtain improved workability, which was favorable for producing a compact and dense matrix with high early strength.

When the H_2O/MK ratio was increased to 0.5, the three geopolymer pastes all displayed improved workability, with yield stress values of 100 to 200 Pa for all pastes at this water content. Similarly to the H_2O/MK = 0.4 series, the geopolymer paste with the most Al species in its activating solution (A2-0.5) had the lowest yield stress. However, for this set of samples at high water content, the addition of Al to the activator can evidently lower the yield stress of the fresh geopolymer paste while maintaining the viscosity, as seen by the fact that the flow curves for all three -0.5 series samples in Figure 2 are parallel at moderate to high shear rate.

3.1.2 Macroscopic fluidity and setting time

It is well known that the fluidity of cement paste is mainly influenced by water usage (i.e., the

water-to-cement ratio in conventional cements). Figure 3a compares the flows (in terms of the diameter spread on a glass plate in a mini slump test) of the geopolymer pastes with varying aluminum contents, at a fixed H_2O/MK ratio of 0.4. The flow increased significantly with the Al/P ratio in the activating solutions. An Al/P ratio of 0.3 led to an increase of the flow diameter by 50% (106 mm) as compared to the reference case of Al/P=0, whose flow diameter was just 78 mm in 60 s. Dividing the flow more specifically into faster and slower processes (i.e., distinguishing yield stress control from viscous control), the fluidity in the first period between 0 and 30 s dominated in the flow test, consistent with the moderate yield stress but relatively low plastic viscosity observed in Figure 2 for each of these pastes. The flow diameter of paste A2 reached about 92 mm, whereas that reached by paste A0 during this period was only 58 mm. However, an opposite trend was observed from 30 to 60 s, whereby the flow diameter for A0 further increased by 19 mm and that for A2 increased by 14 mm. These results indicate that the involvement of aluminum species greatly improved the macroscopic fluidity.

Achieving a reasonable setting time is critical to engineering applications of any cement to be used at ambient temperature. The setting results shown in Fig. 3b demonstrate the difference between the geopolymers with and without the added aluminum species. In the early period, slow dealumination from the MK particles occurred when encountering the activating solution to form an inter-grain gel [32]. The initial setting of the geopolymer pastes stemmed from the free aluminum species combining with phosphate to form an aluminophosphate gel [28]. Therefore, the long initial setting time in geopolymer A0 might be a result of the release of aluminum into solution from the solid aluminosilicate source (i.e., the dealumination reaction) delaying its hardening, whereas feeding aluminum directly in the activating solution could provide the necessary aluminum in the early stages of reaction without the need to wait for the solid precursor to dissolve to such an extent. Thus, as shown in the results for mixes A1 and A2 (Fig. 3b), the free aluminum species in the activating solution could drive a rapid sol/gel transition due to the supplementation of the free Al in the aqueous phase providing the opportunity for near-immediate gel formation. The initial setting times reached a range suitable for engineering applications, although the initial setting time was still rather long (about 3 h). Nevertheless, the free aluminum species, whether supplied from either the activating solution or the solid aluminosilicate source, controlled the reaction rate and affected the setting time of the geopolymer pastes.

3.1.3 Liquid-state ^{31}P and ^{27}Al NMR of phosphate activators

Figures 4a and 4b show the liquid-state ^{31}P and ^{27}Al NMR spectra, respectively, of the MAP solution and the two activating solutions mixed with different Al contents, to further explain the experimental results for the fresh geopolymer pastes. From the ^{31}P spectra for all three solutions (Fig. 4a), three distinct bands at 0 to -1.5 ppm, -8 to -9 ppm, and -12 to -14 ppm were detected, and attributed to Q^0, Q^1 and Q^2 phosphate structural units, respectively [33]. The orthophosphate group (i.e., phosphoric acid molecules and ions [34]) generates the phosphorus environment of Q^0, while the two clear signals resonated between -5 to -24 ppm are due to polyphosphates – either sites with P-O-P linkages (-7~-9 ppm), or Al complexed to phosphate-containing ligands (-12~-14 ppm) [34-36]. The band assigned to P-O-P linkages is caused by the species $[Al(L)]^{m+}$ (where L is H-bonded polymeric OPA, such as $H_6P_2O_8$), while the band centered at a chemical shift of around -13 ppm is associated to the species of $[Al(H_2O)_5(H_2PO_4)]^{2+}$ and trans-$[Al(H_2O)_4(H_2PO_4)_2]^{+}$ as a result of ionic bonding between Al and P [37]. Since the A1 solution was prepared by using small dosage of the MAP solution to dilute the OPA for a resulting Al/P molar ratio of 0.1, the spectrum of the A1 solution in Fig. 4a is embodied by a sharp resonance peak at -0.5 ppm and two small resonances at -8 and -13 ppm. This indicates that the Q^0 phosphate structural unit is dominated in the A1 activating solution with marginal Q^1 and Q^2 phosphate structural units. Similarly, the A2 activating solution prepared by a higher ratio of MAP/OPA (Al/P molar ratio is 0.3) contains more Q^0 and Q^2 phosphate structural units but little Q^1 phosphate structural unit. The addition of Al to adjust the Al/P ratio did not change the chemical environmental of phosphorus when the molar ratio of aluminum to phosphorus was less than 1.0 [34]. However, an increase in the intensity of the band at -8 ppm with decreasing Al content is observed. The resonances assigned to aluminophosphate oligomers (i.e., -12 ~-14 ppm) are intensified (enriched and broadened) with increasing Al content in phosphate activators, which is the result of chemical exchanges between Al and P. This chemistry can break the long phosphate chains (P-O-P linkages) and decrease the polymerization degree [34, 37]. The oligomers formed as a result of the chain breakage benefit the workability of the geopolymer paste, as measured via yield stress and viscosity (in Fig. 2) and fluidity (in Fig. 3.1a).

The resonances that are evident in the ^{27}Al spectra at around -8 ppm, and between 80 to 65 ppm, were due to the aluminum species in MAP, in which a clear hexa-coordinated environment of aluminum (i.e., -1 to -9 ppm) was identified (Fig. 4b) [34, 38]. It has previously been reported that the hexa-coordinated aluminum species is the main form of Al in a hardened phosphate-

activated geopolymer [39]. This is consistent with the addition of Al to the activating solution accelerating the early stage of the geopolymerization process (formation of aluminate and phosphate oligomers) under an acidic phosphate environment, thus leading to a shortened setting time. A weak, broad resonance at 80 to 65 ppm can be attributed to a small quantity of tetrahedral aluminum present under these conditions [40]. These results indicated that in this pH range (i.e., below 2.0, see Table 1) the OPA did not change the hexa-coordinated Al environment seeded by the MAP. However, as observed in the ^{31}P NMR spectra, the intensity and breadth of the bands resonating at 0 to -20 ppm increase with Al contents in the phosphate activators, which can be attributed to the chemical bonding between Al and P species to form low polymeric units [37].

3.2 Hardened geopolymer paste

3.2.1 Compressive strength

As displayed in Fig. 5, the hardened geopolymer pastes prepared with varying Al/P ratios showed significant differences in strength development from 3 to 28 d. In the early stage at 3 and 7 d, the existence of soluble aluminum species in the activating solution caused significant enhancement of the compressive strength. Compared with mix A0 (Al/P=0), mix A2 (Al/P=0.3) showed strengths that were higher by 14.1 MPa and 15.1 MPa at 3 and 7 d, respectively. Geopolymer A2 remained almost the same strength from 7 d up to 28 d. In comparison, the most significant increase in the compressive strength was achieved in geopolymer A0 (with no aluminum species in the activating solution), which evolved from 22.1 MPa at 7 d to 51.3 MPa at 28 d. The strength of the geopolymer A1 (Al/P=0.1) was moderately improved at both 3 and 7 d, but the strength growth thereafter was inferior to that of geopolymer A0. It seems that the hardening during the early period caused by the addition of free aluminum species in the activating solution can compromise or hinder the ongoing reaction of MK (involving dealumination and delamination to provide nutrients for gel growth) in the latter period. Therefore, a tradeoff was found between the early-state strength and the long-term strength, depending on the content of Al in the activating solution.

3.2.2 X-ray diffraction

The XRD patterns of the 28 d hardened geopolymers shown in Fig. 6 indicate that no new

crystalline phase was generated in this reaction process. The only distinct peak in any of the diffractograms is assigned to the quartz that was already present in the unreacted MK particles. The geopolymerization of aluminosilicates, regardless of the activation approach (either by alkali or phosphate activation), involves the dissolution and reconstruction of aluminates and silicates to form disordered gels [41, 42]. In Fig. 6a, a visible difference between the geopolymers and the MK is the change in the broad diffuse peak at 15º to 30º (2θ), whose enlarged view is shown in Fig. 6b. It can be seen that the diffuse peak partially disappears and shifts after the reaction, especially for geopolymer A0. For geopolymers A1 and A2, the diffuse peak is weakened and shows much less intensity in the range 22º to 26º (2θ) compared with that of the MK particles. Similar findings were reported by Cui et al. [16], Douiri et al. [42], and Louati et al. [12], although they all used H_3PO_4 without additional Al to activate the aluminosilicate precursors for synthesis of silico-aluminophosphate geopolymers. These spectral changes can be attributed to the effect of phosphate activation on the MK particles. Considering the XRD pattern of MK as a reference, a larger diffuse peak change (at 18 to 28º) in geopolymer A0 than that in the other geopolymers indicates that the degree of reaction of the MK particles in geopolymer A0 was higher than that of the others at 28 d, consistent with the compressive strength data and confirming that the addition of free aluminum species into geopolymers A1 and A2 may, to some extent, hinder the ongoing reaction of MK in the latter period of curing.

3.2.3 Thermogravimetry

The thermogravimetric/differential thermal analysis (TG-DTA) thermograms for the hardened geopolymer pastes, normalized to the basis of constant mass of MK, are shown in Fig. 7. For all geopolymers, four distinct groups of decomposition or phase transition peaks are observed in the DTA curve: one is located between 100 and 150 ºC, and the others are located in the ranges of 160 to 230 ºC, 800 to 840 ºC, and 980 to 1010 ºC.

The weight loss at 100 to 150 ºC, accompanied by a sharp endothermic peak in the DTA curves, is attributed to the removal of physically adsorbed water and the dehydration of some of the water-containing gels (loss of loosely chemically bonded water), which accounted for more than 80% of the total weight loss. The subsequent weight loss from 150 to 1050 ºC is marginal in each geopolymer, and largely parallels the TGA curve of the MK; this is attributed mainly to dehydration and dehydroxylation of remnant MK particles within the hardened binder, with a

potential minor contribution from any remaining chemically bound water in the reaction product gels.

The features at 160 to 230 ºC and 800 to 870 ºC, respectively, show exotherms in the DTA data but no notable corresponding mass loss, and so are likely to relate to phase transitions in the newly formed binder gel. These may be assigned to the amorphous aluminum phosphate phase transforming into trigonal (α-$AlPO_4$) and tetragonal (β-$AlPO_4$) berlinite at elevated temperature [43], which is an exothermic process. These two peaks were not detected in the MK particles. The last phase transition was the formation of mullite from residual, fully dehydroxylated MK particles at 980 to 1010 ºC [44], and is especially prominent in the raw MK particles. For all geopolymer samples, such a peak is less significant, indicating that the raw MK particles had reacted with the phosphate activating solution to synthesize new gels: silico-alumino-phosphate (S-A-P) gel [16] and amorphous or semi-crystalline aluminum phosphate compounds [12, 17]. The presence of similar peaks representing thermally induced processes in all of the geopolymers reveals that there were similar reaction products regardless of the Al/P ratio of the activating solutions. In other words, the compositions of the resulting gels were not strongly influenced by changes in the activating solution with different Al/P ratios.

3.2.4 Microstructure

However, the pore structures of the geopolymer products did exhibit notable differences when the level of soluble aluminum species was varied (Fig. 8). The MIP results indicate that the porosity of the geopolymer pastes cured for 28 d increased with the Al/P ratio of the activating solutions used, from 17.1% in geopolymer A0 to 18.9% in geopolymer A1 and 21.5% in geopolymer A2 (Fig. 8a). This porosity result is in agreement with the trend in their strength behaviors (i.e., a higher-strength matrix showed lower porosity). The pore diameters accessible to mercury were mainly concentrated between 5 and 1000 nm (Fig. 8b), and can be divided into gel pores (less than 10 nm), small capillary pores (10 to 50 nm), medium capillary pores (50 to 100 nm) and large capillary pores (100 to 10 μm) [45-47]. Fig. 8c shows the differential pore diameter distributions and the diameter range between 10 and 1000 nm is enlarged in Fig. 8d. It can be seen for all geopolymers that the capillary pores (small, medium, and large) contributed more than 90% of the porosity. However, the incorporation of aluminum species in the activating solution changed the distribution characteristics of the capillary pores. An increase in the Al content of the activating solution led to a shift to larger capillary pores. The

pore size distribution of the geopolymer with the most soluble aluminum (i.e., A2 with an Al/P ratio of 0.3) exhibited a sharp maximum at around 90 nm. The other geopolymer samples (A0 and A1) showed similar differential porosity distributions to each other, with peak values at 60 nm and 73 nm, respectively. These different distributions of the capillary pores will eventually govern the strength and transport properties of the geopolymer matrix. A delayed or compromised dealumination reaction of the metakaolin particles is more likely to produce discontinuous gels that generate inter-gel spaces which form medium and large capillary pores.

The features identified through this analysis of pore structure are supported by the morphologies and elemental analysis obtained by SEM and EDS. Fig. 9 shows SEM results for the hardened geopolymer pastes cured at 3 d. As shown in Fig. 9a, the A0 matrix consisted of many isolated particles intermixed with gel-like lumps. In the image with higher magnification (Fig. 9b), some discontinuous phases and micro cracks are found, implying a weak reaction between MK and Al-free activators at the early period. The EDS analysis (Fig. 10) indicates the presence of different Al:Si:P ratios at different locations. For instance, points 1 and 2 corresponded to the unreacted MK particles (aluminosilicates without P) and the newly-formed S-A-P gels (reaction products), respectively. As a comparison, the presence of soluble aluminum species in the phosphate activator led to a more compact matrix after the 3 d curing process (in Fig. 9c), although such curing was insufficient for geopolymerization between the MK particles and the activating solution. The enlarged image of the A2 geopolymer cured at 3 d (Fig. 9d) shows a high-continuity texture without isolated phases and micro cracks. The EDS analysis for the compact area (i.e., area 1 in Fig. 9c and Fig. 10) reveals the presence of Si, Al and P, which is very likely to be the result of S-A-P gel formation. However, compared to the EDS spectrum of Point 2, a lower silicon content in this gel indicates that the presence of soluble Al and P species may form aluminophosphate gels for early strength improvement (Fig. 5).

The morphologies of the three geopolymer samples imaged at 28 d revealed that the use of excessive aluminum species (A2, shown in Fig. 11c) was unfavorable due to the production of discontinuous gels as compared with A0 (Fig. 11a). Geopolymer A1 with a moderate content of soluble aluminum species (Fig. 11b) seemed to present an intermediate state between A0 and A2. These microstructural observations coincided well with the strength variation and development of the three geopolymer matrices as discussed above, where the longer-term strength evolution of A2 beyond 7 days was negligible while A0 continued to gain more strength.

4. Conclusions

The effects of the addition of soluble aluminum species into a phosphate activating solution for geopolymer synthesis on fresh and hardened properties were investigated in terms of workability, compressive strength, and the microstructure.

The incorporation of aluminum species into the phosphate activating solution allowed a rapid sol/gel transition in the early state due to the supplementation of the free Al (in six-coordination). As a result, the fresh geopolymer paste achieved good workability. The role of aluminum species was similar to that of a plasticizer, lowering the yield stress of the fresh geopolymer paste while keeping the viscosity unchanged. As a result, a compact and dense matrix was obtained with a high early strength of up to 37 MPa at 7 d of curing.

However, the use of soluble aluminum species may also lead to relatively poor strength development in the latter stage depending on the added dose. A geopolymer with an excessive amount of aluminum species may exhibit significant inter-gel spaces (medium capillary pores) due to the formation of discontinuous gels and inability to close and refine these pores at later age, because the accelerated hardening and gel formation blocks the unreacted MK particles and hinders their dealumination reaction.

Acknowledgements

The authors would like to acknowledge the financial support received from the Research Grants Council of the Hong Kong SAR (Project No. PolyU 5145/13E), the National Science Foundation of China (NSFC) Project No. 51638008, and the Hong Kong Polytechnic University through its Ph.D. studentship. The first author would also like to thank the University of Sheffield for hosting a 3-month exchange visit.

References

[1] Davidovits, J. (1991). Geopolymers: Inorganic polymeric new materials. *Journal of Thermal Analysis*, **37**: 1633-1656.

[2] Ismail, I., Bernal, S. A., Provis, J. L., San Nicolas, R., Hamdan, S., & van Deventer, J. S. J.

(2014). Modification of phase evolution in alkali-activated blast furnace slag by the incorporation of fly ash. *Cement and Concrete Composites*, **45**, 125-135.

[3] Juenger, M. C. G., Winnefeld, F., Provis, J. L., & Ideker, J. H. (2011). Advances in alternative cementitious binders. *Cement and Concrete Research*, **41**(12), 1232-1243.

[4] Provis, J. L., Palomo, A., & Shi, C. (2015). Advances in understanding alkali-activated materials. *Cement and Concrete Research*, ***78***, 110-125.

[5] Ouellet-Plamondon, C., & Habert, G. (2015). Life cycle assessment (LCA) of alkali-activated cements and concretes. In *Handbook of alkali-activated cements, mortars and concretes*, pp. 663-686.

[6] Ding, Y., Dai, J. G., & Shi, C. J. (2016). Mechanical properties of alkali-activated concrete: a state-of-the-art review. *Construction and Building Materials*, **127**, 68-79.

[7] Provis, J. L. & van Deventer, J. S. J. (2014). *Alkali-activated materials: state-of-the-art report, RILEM TC 224-AAM*. RILEM/Springer, Dordrecht.

[8] Provis, J. L. & Bernal, S. A. (2014). Geopolymers and related alkali-activated materials. *Annual Review of Materials Research*, **44**(1), 299-327.

[9] Wagh, A. S. (2005). Chemically bonded phosphate ceramics—a novel class of geopolymers. *Ceramic Transactions*, **165**, 107-116.

[10] Davidovits, J. (2011). *Geopolymer: chemistry & applications, 3rd edition*. Geopolymer Institute, Saint-Quentin.

[11] Louati, S., Baklouti, S., & Samet, B. (2016). Acid based geopolymerization kinetics: Effect of clay particle size. *Applied Clay Science*, **132**, 571-578.

[12] Louati, S., Hajjaji, W., Baklouti, S., & Samet, B. (2014). Structure and properties of new eco-material obtained by phosphoric acid attack of natural Tunisian clay. *Applied Clay Science*, **101**, 60-67.

[13] Wang, Y. S., Dai, J. G., Ding, Z. & Xu, W. T. (2017). Phosphate-based geopolymer: Formation mechanism and thermal stability. *Materials Letters*, **190**, 209-212.

[14] Cao, D., Su, D., Lu, B., & Yang, Y. (2005). Synthesis and structure characterization of geopolymeric material based on metakaolinite and phosphoric acid. *Journal of the Chinese Ceramic Society*, **33**: 1385-1389.

[15] Liu, L. P., Cui, X. M., Qiu, S. H., Yu, J. L. & Zhang, L. (2010). Preparation of phosphoric acid-based porous geopolymers. *Applied Clay Science*, **50**: 600-603.

[16] Cui, X. M., Liu, L. P., He, Y., Chen, J. Y., & Zhou, J. (2011). A novel aluminosilicate geopolymer material with low dielectric loss. *Materials Chemistry and Physics*, **130**(1-2), 1-4.

[17] Derouane, E.G., Fripiat, J.G. and von Ballmoos, R. (1990). Quantum mechanical calculations on molecular sieves. 2. Model cluster investigation of silicoaluminophosphates. *Journal of Physical Chemistry*, **94**(4): 1687-1692.

[18] Zhang, Z., Provis, J. L., Reid, A., & Wang, H. (2014). Fly ash-based geopolymers: the relationship between composition, pore structure and efflorescence. *Cement and Concrete Research*, **64**, 30-41.

[19] Kovalchuk, G., Fernández-Jiménez, A., & Palomo, A. (2007). Alkali-activated fly ash: effect of thermal curing conditions on mechanical and microstructural development–Part II. *Fuel*, **86**(3), 315-322.

[20] Marjanović, N., Komljenović, M., Baščarević, Z., Nikolić, V., & Petrović, R. (2015). Physical–mechanical and microstructural properties of alkali-activated fly ash–blast furnace slag blends. *Ceramics International*, **41**(1), 1421-1435.

[21] Bernal, S. A., San Nicolas, R., Van Deventer, J. S. J., & Provis, J. L. (2016). Alkali-activated slag cements produced with a blended sodium carbonate/sodium silicate activator. *Advances in Cement Research*, **28**(4), 262-273.

[22] Gualtieri, M. L., Romagnoli, M., Pollastri, S., & Gualtieri, A. F. (2015). Inorganic polymers from laterite using activation with phosphoric acid and alkaline sodium silicate solution: mechanical and microstructural properties. *Cement and Concrete Research*, **67**, 259-270.

[23] Douiri, H., Kaddoussi, I., Baklouti, S., Arous, M., & Fakhfakh, Z. (2016). Water molecular dynamics of metakaolin and phosphoric acid-based geopolymers investigated by impedance spectroscopy and DSC/TGA. *Journal of Non-Crystalline Solids*, **445**, 95-101.

[24] He, Y., Liu, L., He, L., & Cui, X. (2016). Characterization of chemosynthetic H_3PO_4–Al_2O_3–$2SiO_2$ geopolymers. *Ceramics International*, **42**(9), 10908-10912.

[25] Duxson, P., Provis, J. L., Lukey, G. C., Mallicoat, S. W., Kriven, W. M., & Van Deventer, J. S. J. (2005). Understanding the relationship between geopolymer composition, microstructure and mechanical properties. *Colloids and Surfaces A: Physicochemical and Engineering Aspects*, **269**(1-3), 47-58.

[26] Jansson, H., Bernin, D., & Ramser, K. (2015). Silicate species of water glass and insights for alkali-activated green cement. *AIP Advances*, **5**(6), 067167.

[27] Benavent, V., Steins, P., Sobrados, I., Sanz, J., Lambertin, D., Frizon, F., Rossignol, S., & Poulesquen, A. (2016). Impact of aluminum on the structure of geopolymers from the early stages to consolidated material. *Cement and Concrete Research*, **90**, 27-35.

[28] Petzet, S., Peplinski, B., Bodkhe, S. Y., & Cornel, P. (2011). Recovery of phosphorus and aluminium from sewage sludge ash by a new wet chemical elution process (SESAL-Phos-

recovery process). *Water Science and Technology*, **64**(3), 693-699.

[29] Roussel, N., Lemaître, A., Flatt, R. J., & Coussot, P. (2010). Steady state flow of cement suspensions: a micromechanical state of the art. *Cement and Concrete Research*, **40**(1), 77-84.

[30] Dai, J. G., Munir, S., & Ding, Z. (2013). Comparative study of different cement-based inorganic pastes towards the development of FRIP strengthening technology. *Journal of Composites for Construction*, **18**(3), A4013011.

[31] Favier, A., Hot, J., Habert, G., Roussel, N., & d'Espinose de Lacaillerie, J. B. (2014). Flow properties of MK-based geopolymer pastes. A comparative study with standard Portland cement pastes. *Soft Matter*, **10**(8), 1134-1141.

[32] Favier, A., Habert, G., d'Espinose de Lacaillerie, J. D., & Roussel, N. (2013). Mechanical properties and compositional heterogeneities of fresh geopolymer pastes. *Cement and Concrete Research*, **48**, 9-16.

[33] Chavda, M. A., Bernal, S. A., Apperley, D. C., Kinoshita, H., & Provis, J. L. (2015). Identification of the hydrate gel phases present in phosphate-modified calcium aluminate binders. *Cement and Concrete Research*, **70**, 21-28.

[34] Samadi-Maybodi, A., Nejad-Darzi, S. K. H., & Bijanzadeh, H. (2009). ^{31}P and ^{27}Al NMR studies of aqueous (2-hydroxyethyl) trimethylammonium solutions containing aluminum and phosphorus. *Spectrochimica Acta Part A: Molecular and Biomolecular Spectroscopy*, **72**(2), 382-389.

[35] Abdi, D., Cade-Menun, B. J., Ziadi, N., & Parent, L. É. (2014). Long-term impact of tillage practices and phosphorus fertilization on soil phosphorus forms as determined by ^{31}P nuclear magnetic resonance spectroscopy. *Journal of Environmental Quality*, **43**(4), 1431-1441.

[36] Liu, J., Yang, J., Liang, X., Zhao, Y., Cade-Menun, B. J., & Hu, Y. (2014). Molecular speciation of phosphorus present in readily dispersible colloids from agricultural soils. *Soil Science Society of America Journal*, **78**(1), 47-53.

[37] Mortlock, R. F., Bell, A. T., & Radke, C. J. (1993). Phosphorus-31 and aluminum-27 NMR investigations of highly acidic, aqueous solutions containing aluminum and phosphorus. *Journal of Physical Chemistry*, ***97***(3), 767-774.

[38] Haouas, M., Taulelle, F., & Martineau, C. (2016). Recent advances in application of ^{27}Al NMR spectroscopy to materials science. *Progress in Nuclear Magnetic Resonance Spectroscopy*, **94**, 11-36.

[39] Perera, D. S., Hanna, J. V., Davis, J., Blackford, M. G., Latella, B. A., Sasaki, Y., & Vance,

578 E. R. (2008). Relative strengths of phosphoric acid-reacted and alkali-reacted metakaolin
579 materials. *Journal of Materials Science*, **43**(19), 6562-6566.
580 [40] Mueller, D., Hoebbel, D., & Gessner, W. (1981). ^{27}Al NMR studies of aluminosilicate
581 solutions. Influences of the second coordination sphere on the shielding of aluminium.
582 *Chemical Physics Letters*, **84**(1), 25-29.
583 [41] Provis, J. L., Lukey, G. C., & van Deventer, J. S. J. (2005). Do geopolymers actually contain
584 nanocrystalline zeolites? A reexamination of existing results. *Chemistry of Materials*,
585 **17**(12), 3075-3085.
586 [42] Douiri, H., Louati, S., Baklouti, S., Arous, M., & Fakhfakh, Z. (2014). Structural, thermal
587 and dielectric properties of phosphoric acid-based geopolymers with different amounts of
588 H_3PO_4. *Materials Letters*, **116**, 9-12.
589 [43] Prado-Herrero, P., Garcia-Guinea, J., Crespo-Feo, E., & Correcher, V. (2010). Temperature-
590 induced transformation of metavariscite to berlinite. *Phase Transitions*, **83**(6), 440-449.
591 [44] White, C. E., Provis, J. L., Proffen, T., Riley, D. P., & van Deventer, J. S. J. (2010). Density
592 functional modeling of the local structure of kaolinite subjected to thermal dehydroxylation.
593 *Journal of Physical Chemistry A*, **114**(14), 4988-4996.
594 [45] Zeng, Q., Li, K., Fen-Chong, T., & Dangla, P. (2012). Pore structure characterization of
595 cement pastes blended with high-volume fly-ash. *Cement and Concrete Research*, **42**(1),
596 194-204.
597 [46] Ma, H., Hou, D., & Li, Z. (2015). Two-scale modeling of transport properties of cement
598 paste: Formation factor, electrical conductivity and chloride diffusivity. *Computational*
599 *Materials Science*, **110**, 270-280.
600 [47] Wang, Y. S., & Dai, J. G. (2017). X-ray computed tomography for pore-related
601 characterization and simulation of cement mortar matrix. *NDT & E International*, **86**, 28-
602 35.
603

Tables and Figures

Table 1. Mix proportions of activating solution and phosphate-based geopolymer.

No.	Raw materials by weight ratio					Fresh geopolymer paste	
	Aluminosilicate source	Activating solution					
	MK[a]	OPA[a]	MAP[b]	Water	Initial pH	Soluble Al species (Al/P)	Si/P molar ratio
A0	10	3.60	0	3.46	1.62	0	2.75
A1	10	2.51	1.98	2.86	1.64	0.1	2.75
A2	10	0.36	5.94	1.65	1.69	0.3	2.75
A0-0.5[c]	10	3.60	0	4.46	1.63	0	2.75
A1-0.5[c]	10	2.51	1.98	3.86	1.66	0.1	2.75
A2-0.5[c]	10	0.36	5.94	2.65	1.69	0.3	2.75

[a] Mass fractions of MK and OPA are 97.9% (SiO_2 + Al_2O_3) and 85%, respectively.

[b] Mass concentration of MAP is 61.3% with a P/Al molar ratio of 2.99.

[c] These mixing proportions were provided only for tests of rheological properties. A0-0.5 means the geopolymer A0 is prepared with a H_2O/MK mass ratio of 0.5. A1-0.5 and A2-0.5 are similarly defined.

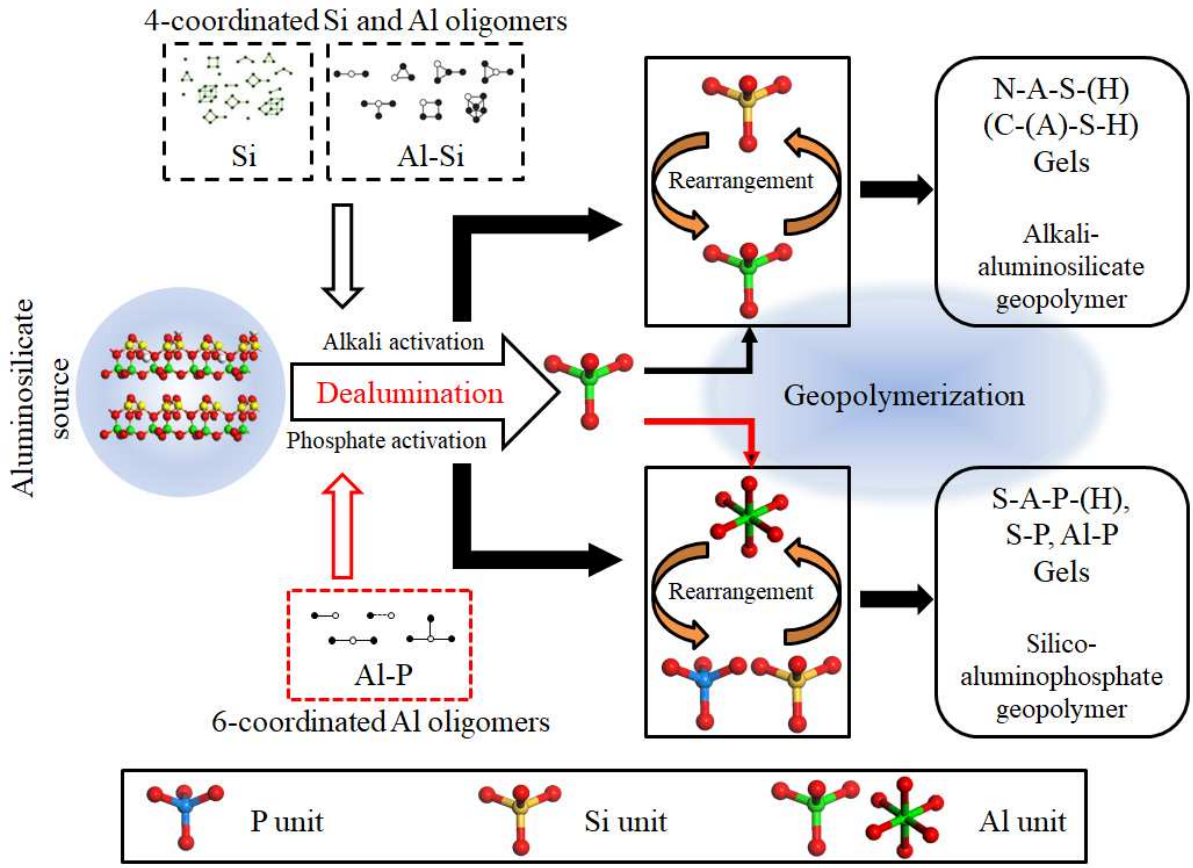

609

610 Fig. 1 Conceptual scheme for an activating solution-accelerated formation process from an
611 aluminosilicate source to a geopolymer. The aluminosilicate source catalyzed by alkali and
612 phosphate synthesizes the respective alkali-aluminosilicate and silico-aluminophosphate
613 geopolymers.

614

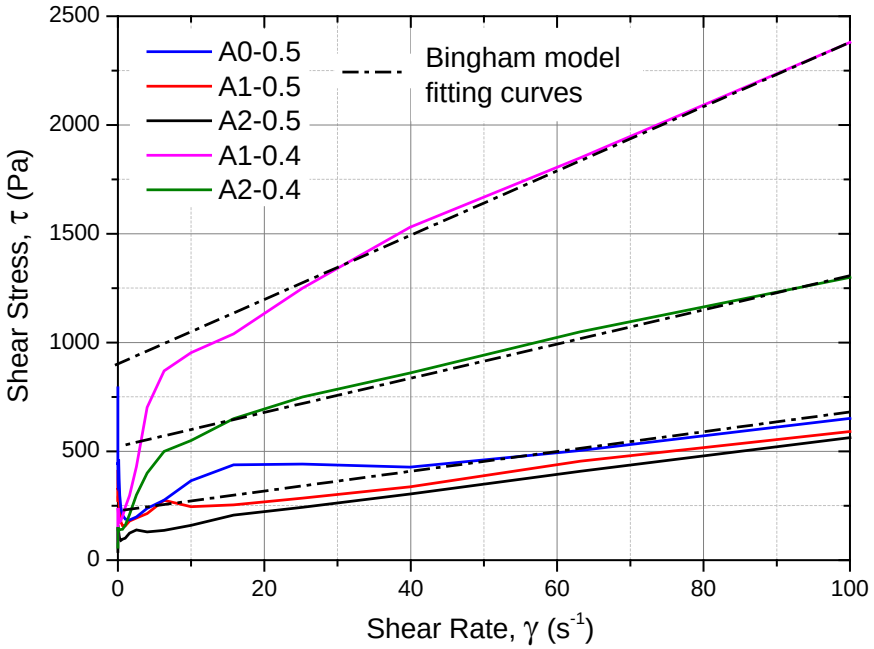

615

616 Fig. 2 Rheological flow curves of the fresh geopolymer pastes with different contents of soluble
617 Al species in their respective activators. The suffix -0.4 or -0.5 in the sample ID indicates the
618 H_2O/MK ratio (0.4 or 0.5). The geopolymer paste prepared using the Al-free activating solution
619 at low water content (i.e., A0-0.4) was outside the measurement range of the rheometer.

620

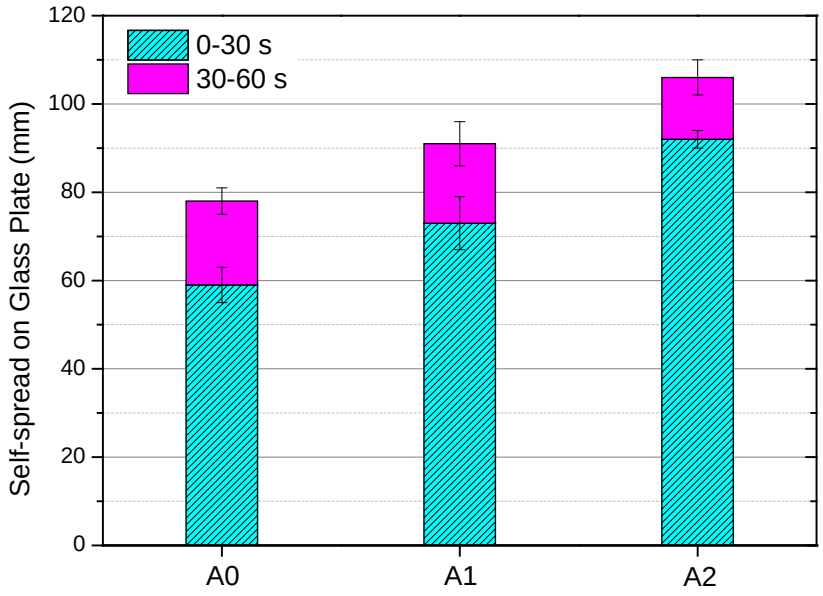

(a)

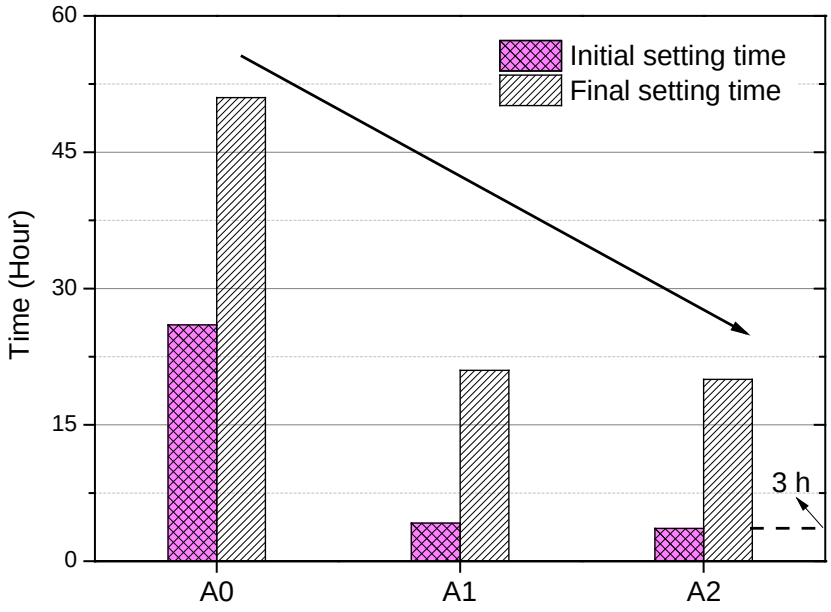

(b)

Fig. 3 Fluidity and setting times of the phosphate-based geopolymer pastes with different contents of soluble Al species. (a) Fluidity. (b) Initial and final setting times.

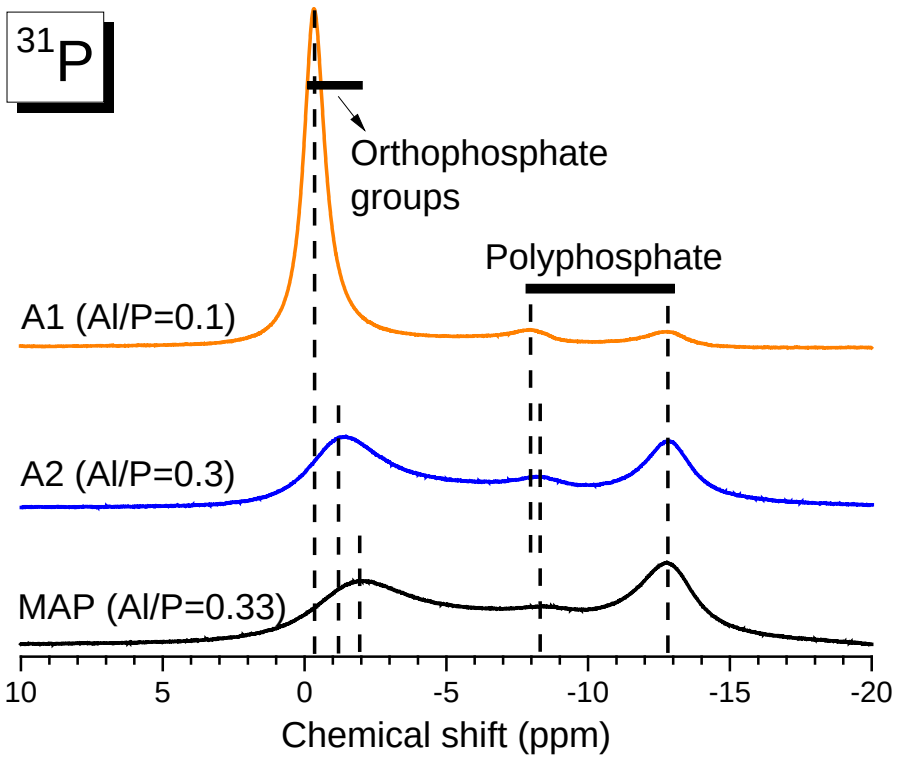

(a)

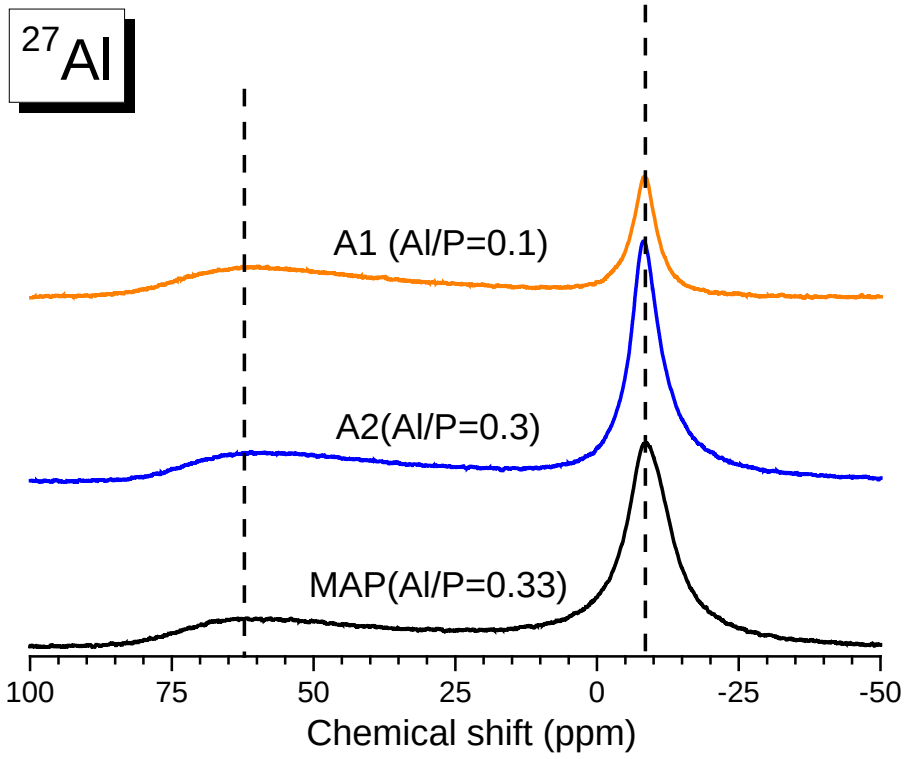

(b)

Fig. 4 Liquid-state ^{31}P and ^{27}Al NMR spectra for the MAP and activating solutions

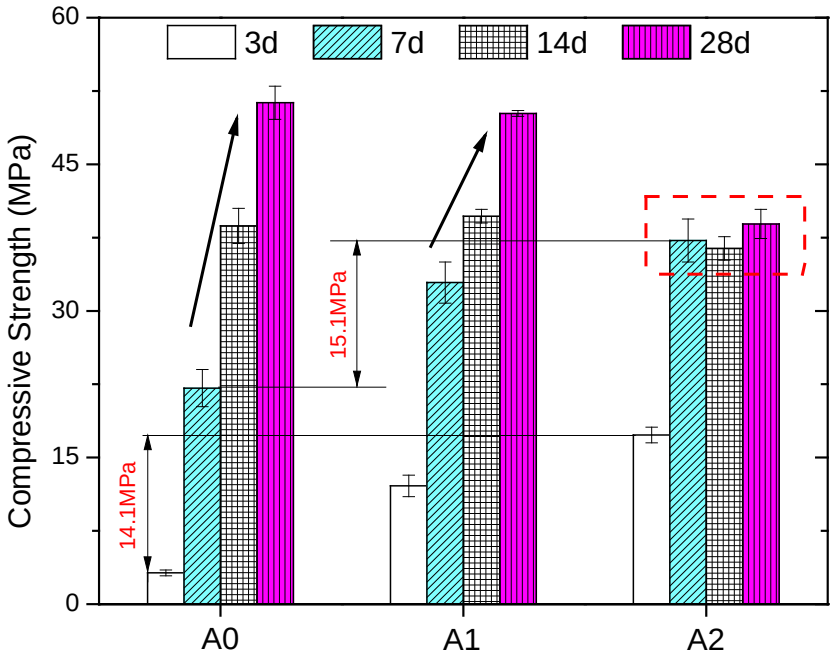

633

634 Fig. 5 Compressive strength development for the first 28 days, of the hardened geopolymer

635 pastes with varying contents of soluble Al species.

636

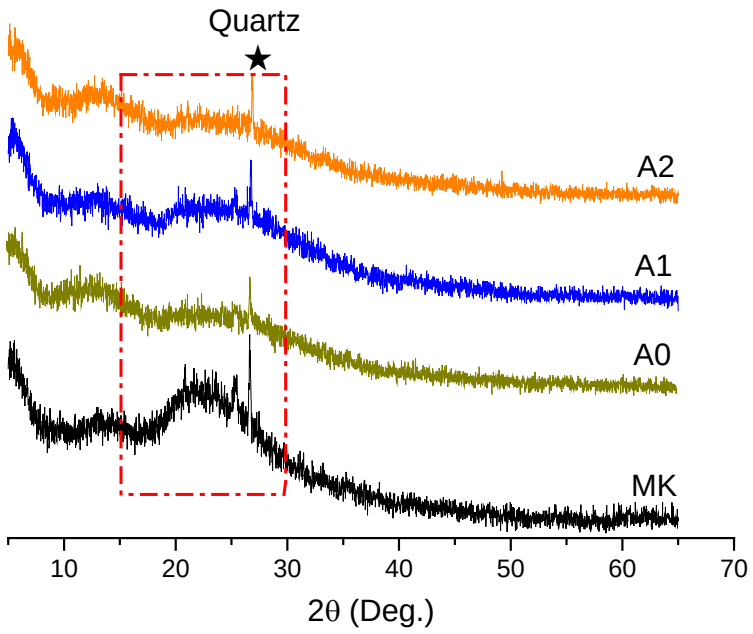

(a)

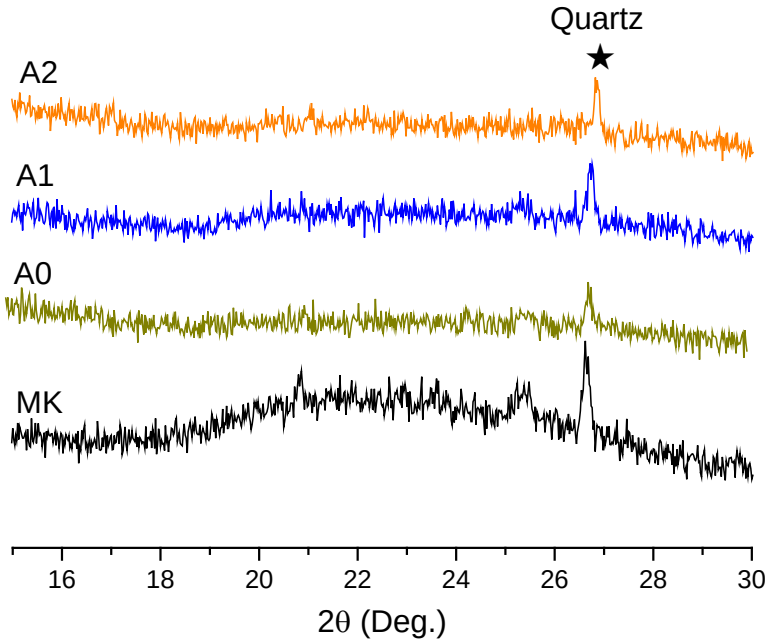

(b)

Fig. 6 XRD patterns of the 28 d cured geopolymers prepared with three different Al/P molar ratios in the activating solution, and the MK precursor. (a) 5º to 65º 2□; (b) enlarged at 15º to 30º 2□.

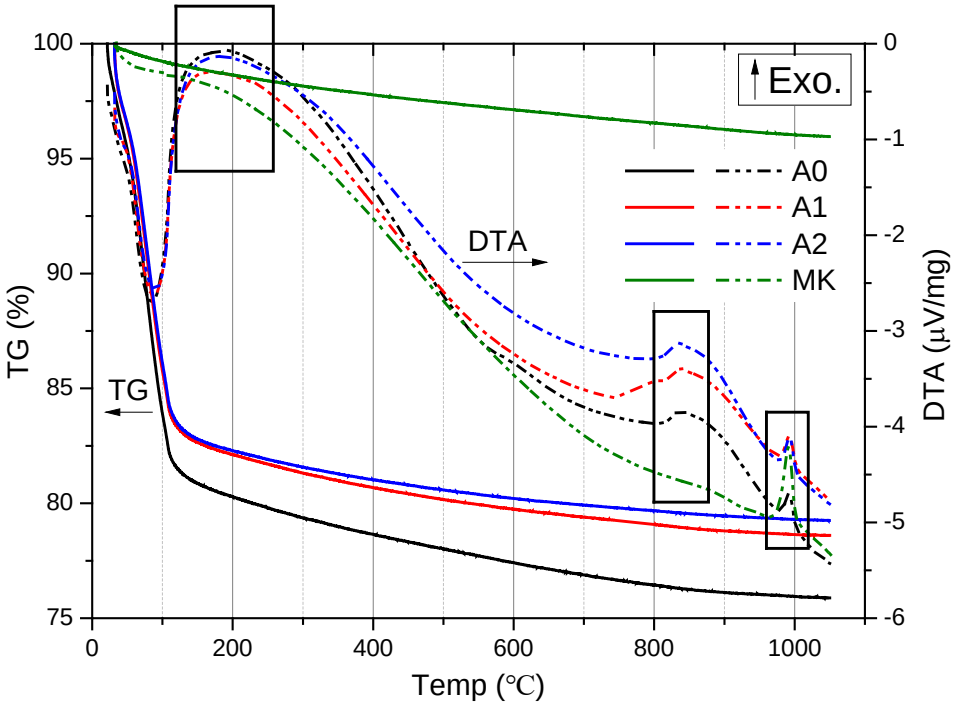

Fig. 7 TG-DTA thermograms for the 28 d cured geopolymers with varying Al/P molar ratios and H_2O/MK ratios.

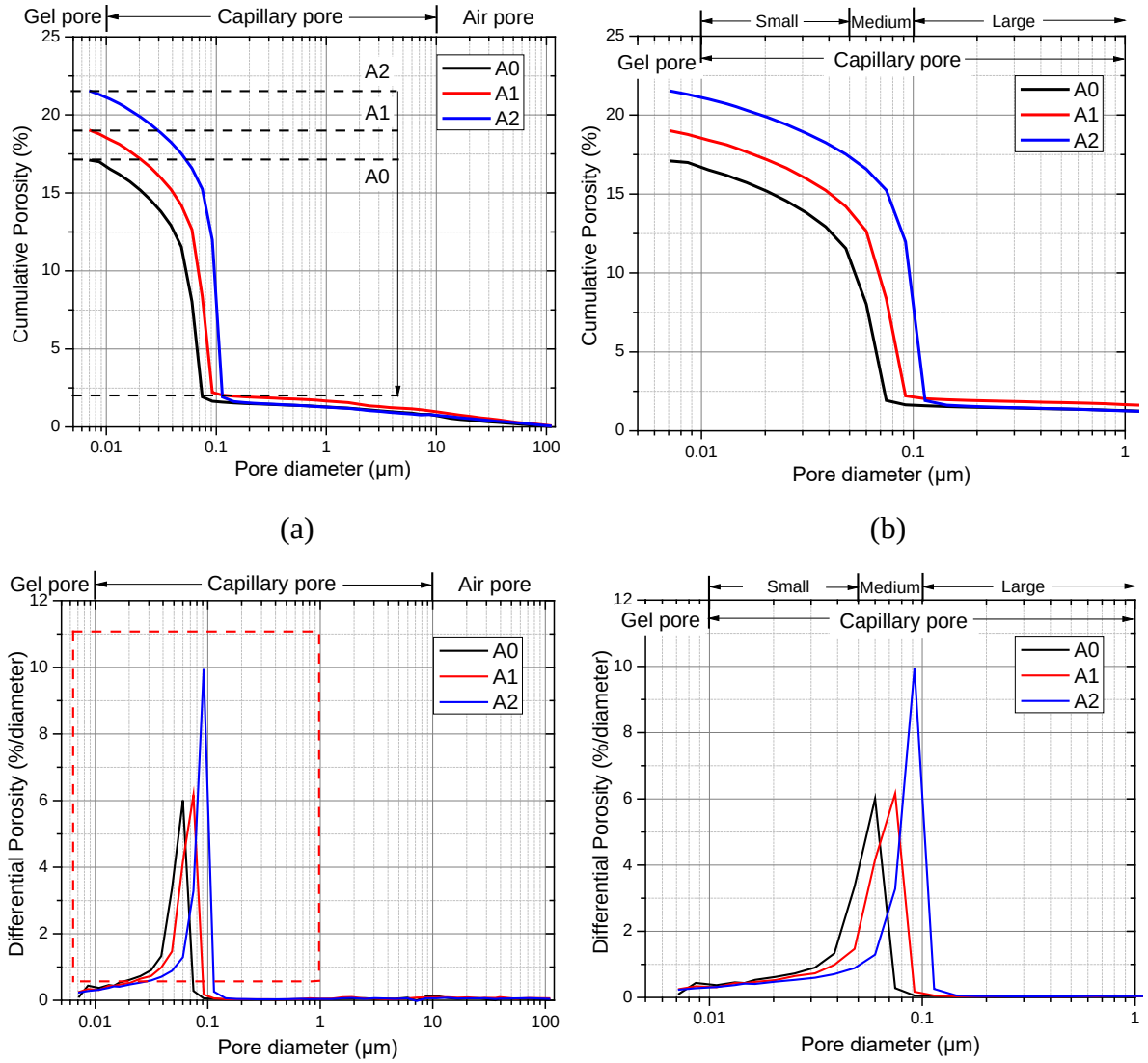

Fig. 8 Pore diameter distributions determined by MIP analysis of the three hardened geopolymer pastes at 28 d. (a, b) Cumulative distribution; (c, d) differential distribution.

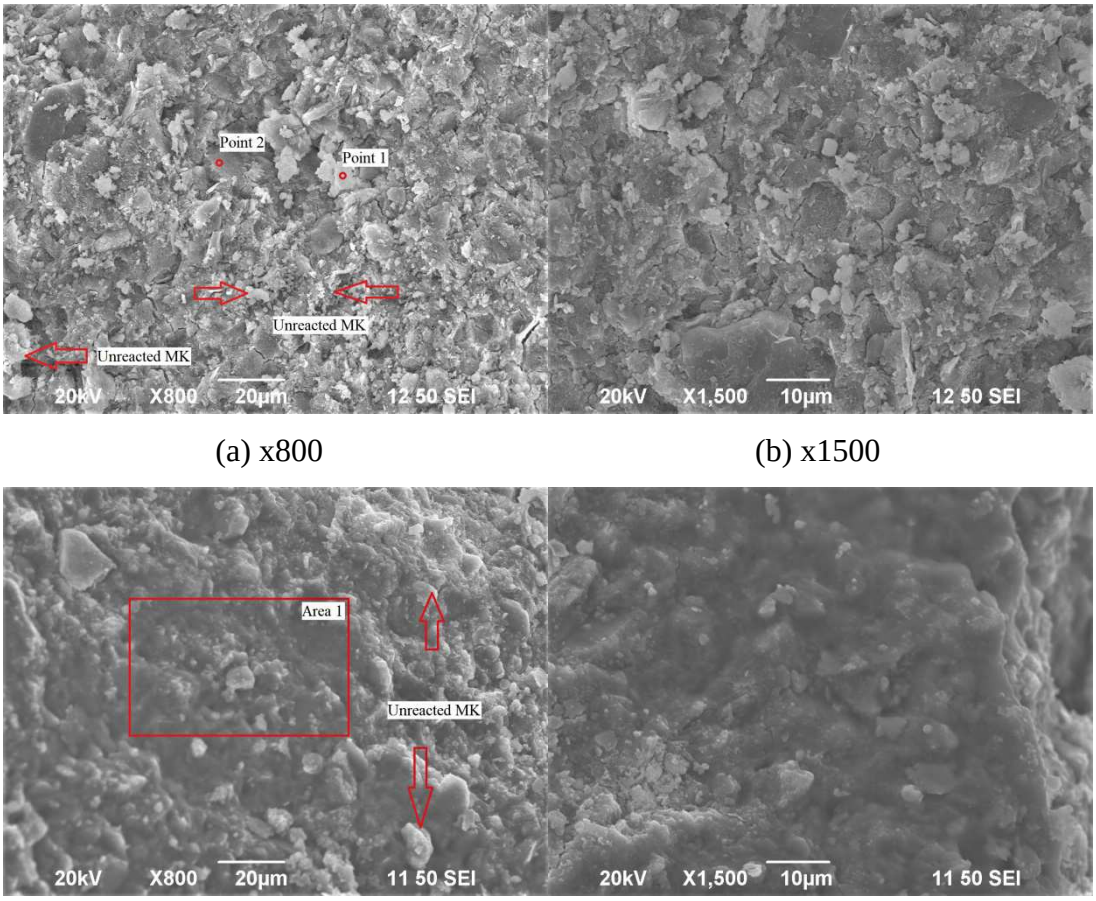

(a) x800 (b) x1500

(c) x800 (d) x1500

Fig. 9 SEM results of the hardened geopolymer pastes cured at 3 d. (a) and (b) A0 geopolymer; (c) and (d) A2 geopolymer.

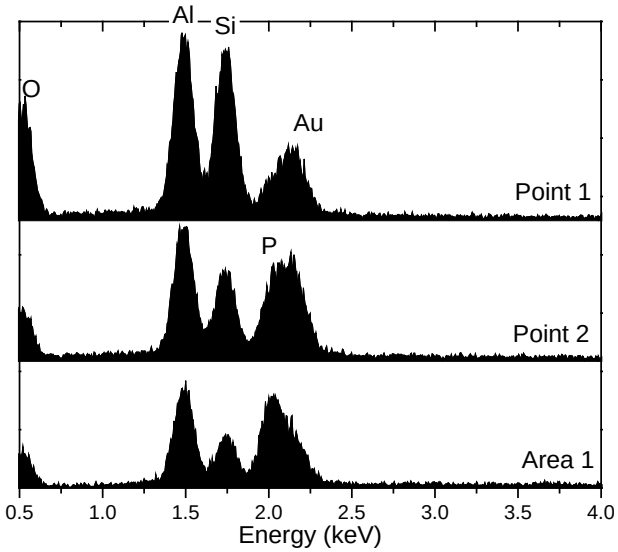

Fig. 10 EDS results of the hardened geopolymer pastes at 3 d. The point 1 point 2 and area 1 can be found in Figs. 9a and 9b.

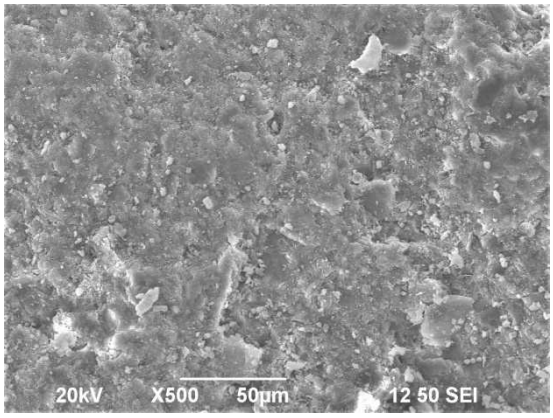

(a)

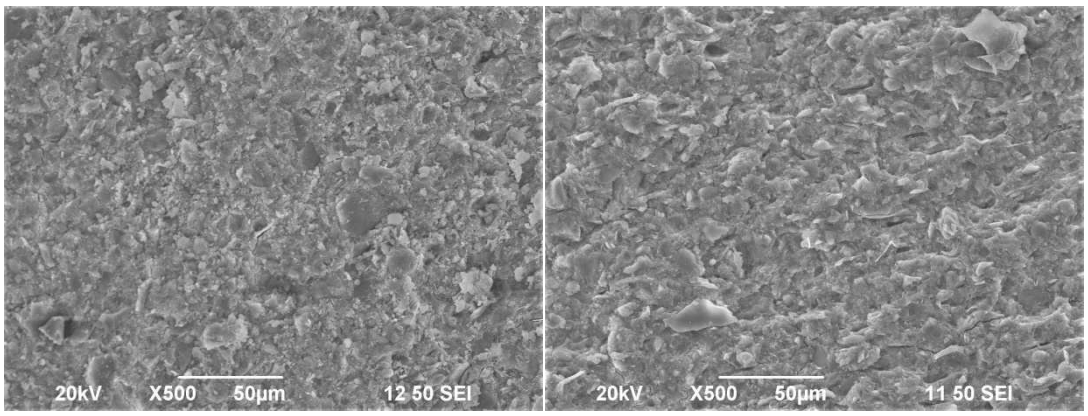

(b) (c)

Fig. 11 SEM results of the hardened geopolymer pastes cured at 28 d. (a) A0 geopolymer; (b) A1 geopolymer; and (c) A2 geopolymer.